Chinese Chemical Letters 37 (2026) 111864

Contents lists available at ScienceDirect

Chinese Chemical Letters

journal homepage: www.elsevier.com/locate/cclet

Chiral porous liquid D-his-ZIF-8-[Bpy][NTf_2] for capillary gas chromatographic separation

Xiao-Yan Ran[1], Tian-Jian Xiong[1], Yu-Ping Yang, Zong-Hong Luo, Cheng Liu, Yu-Lan Zhu, Jun-Hui Zhang, Bang-Jin Wang, Sheng-Ming Xie*, Li-Ming Yuan

Yunnan Key Laboratory of Modern Separation Analysis and Substance Transformation, College of Chemistry and Chemical Engineering, Yunnan Normal University, Kunming 650500, China

ARTICLE INFO

Article history:
Received 18 April 2025
Revised 31 July 2025
Accepted 18 September 2025
Available online 18 September 2025

Keywords:
Chiral porous liquid
Chiral stationary phase
Chiral separation
Gas chromatography

ABSTRACT

Porous liquids (PLs), as a new class of porous materials with permanent porosity and liquid fluidity, have attracted extensive research interest due to their excellent physical and chemical properties. Herein, we synthesized a chiral porous liquid D-his-ZIF-8-[Bpy][NTf_2] based on a metal-organic framework (MOF) and used it as a new stationary phase to investigate its separation performance by high-resolution gas chromatography. The porosity of this porous liquid system was verified through Brunauer-Emmett-Teller (BET) and positron (e^+) annihilation lifetime spectroscopy (PALS). The results showed that the D-his-ZIF-8-[Bpy][NTf_2] coated capillary column (column A) exhibited excellent separation performance for n-alkanes, n-alcohols, alkylbenzenes, isomers, and racemic compounds. Among them, fifteen pairs of enantiomers including alcohols, esters, epoxides, ketones, haloalkanes, and amino acid derivatives were well separated on column A with good reproducibility and stability. The relative standard deviations (RSDs) of the retention time and peak area of two analytes (3-butyne-2-ol and dichlorobenzene) were <1.80 % and 0.80 %, respectively. By comparing the chiral recognition ability of D-his-ZIF-8-[Bpy][NTf_2] coated column A with D-his-ZIF-8 coated column B, the column A has better separation efficiency for chiral compounds than column B. In addition, the chiral recognition ability of column A is complementary to that of commercially available β-DEX 120 column (column C). Compared with the commercial HP-35 column and the previously reported P5A-C10–2NH_2 column for the separation of organic mixtures and/or isomers, column A exhibits similar separation performance and has a good separation complementarity to these two columns. Hence, this work opens up a new way for the practical application of porous framework solid materials in gas chromatography.

© 2026 Published by Elsevier B.V. on behalf of Chinese Chemical Society and Institute of Materia Medica, Chinese Academy of Medical Sciences.

Porous liquids (PLs) are a new type of material with a stable permanent cavity structure and fluidity that combines the advantages of solid-liquid two-phase flow [1–5]. PLs have the characteristics of regular, permanent, and stable intramolecular cavities, where the cavity size can range from 0.1 nm to 50 nm depending on the pore maker [6–8]. In the last few years, PLs based on various advanced porous solids such as metal-organic frameworks (MOFs), porous organic cages (POCs), metal organic cages (MOCs), porous carbons, zeolites, and porous polymers have been reported [9–14]. The concept of PLs was first proposed by Prof. James in a 2007 paper, which classified PLs into three types [15]. Type I PLs composed of neat liquid hosts that have inherent porosity [16]. Type II PLs mean molecular type porous liquids containing dissolved hollow rigid hosts (*e.g.*, POCs and MOCs) in size-excluded solvents [17,18]. Type III PLs are a type of stable suspensions obtained by dispersing porous materials such as MOFs, COFs, and zeolites in steric hindrance solvents [19–20].

Notably, PLs have the advantages of negligible volatility, high gas solubilities, and adjustable viscosity, which promotes rapid development in the fields of gas adsorption [21–23], chiral separation [24], catalysis [25–28], extraction [29,30], and chiral induction [31]. In 2017, Zheng *et al.* [32] adopted an electrostatic interaction strategy to prepare mesoporous carbon ball liquid with multilevel hollow structures and liquid-like fluidity, demonstrating great potential for gas capture applications. In 2019, Maschmeyer *et al.* [33] studied the catalytic hydrogenation of several alkenes and nitroarenes using Pt nanoparticles encapsulated in type I porous liquid (Pt@HS-SiO_2 PL). The results showed that the Pt@HS-SiO_2 PL catalyst in ethanol has the fastest reaction rate for the hydrogena-

* Corresponding author.
E-mail address: xieshengming_2006@163.com (S.-M. Xie).
[1] These authors contributed equally to this work.

https://doi.org/10.1016/j.cclet.2025.111864
1001-8417/© 2026 Published by Elsevier B.V. on behalf of Chinese Chemical Society and Institute of Materia Medica, Chinese Academy of Medical Sciences.

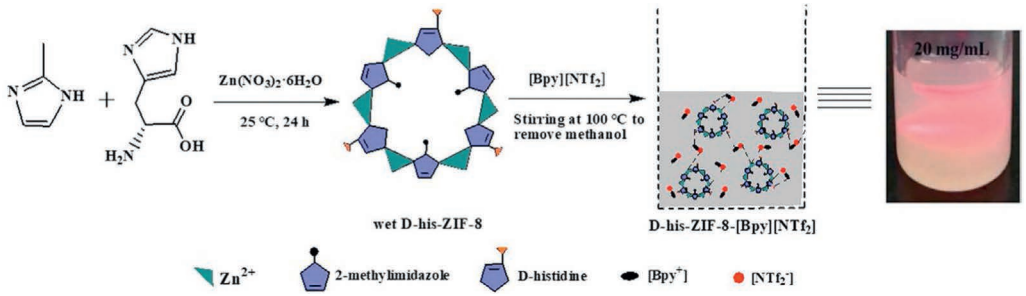


Fig. 1. Schematic diagram for the preparation of D-his-ZIF-8-[Bpy][NTf_2].

tion of 1-decene when normalized with respect to the concentration of Pt. Xia *et al.* [24] reported the effective chiral recognition and separation of nucleosides in solution using cyclodextrin derived type I PL. Zhang *et al.* [17] reported that a type II PL formed by a coordination cage dissolved in trihexyltetradecylphosphonium chloride exhibited extraordinary selectivity for L-tryptophan. Recently, Huang group [30] reported a simple *in-situ* ion thermal synthesis strategy for preparing hybrid monolayers of ionic liquids/MOF (ILs@ZIF-8) nanocomposites to promote efficient capillary microextraction of trace amounts of microcystins in environmental water. These studies not only enrich the design of new PLs, but also make them a good candidate for chromatographic separation applications.

Up to now, many research groups have successfully used porous framework materials (*e.g.*, MOFs and COFs), mesoporous silicas, graphene oxide, and pillararenes for capillary gas chromatography (GC) separation [34–39]. However, the capillary columns prepared based on these materials mainly use dynamic coating or *in-situ* growth methods, which can lead to difficulties in preparing capillary columns and poor column reproducibility [40]. However, the constructing porous framework materials into PLs as stationary phases for GC separation can effectively solve the above problems, while also improving the mass transfer efficiency and separation performance of the stationary phases. It is known from the reported type I PLs that their application is limited in some fields due to the difficulties in synthesis, gel like, high melting point, and low yields [41]. For type II PLs, there have been few research reports due to the drawbacks of high solvent toxicity, non-economy, and limited porous molecular cages (POCs and MOCs) selection [42]. Considering the significant progress and wide selection of porous materials, the type III PLs are the most promising in achieving high porosity, adjustable pore characteristics, and functionalization [43]. As is well known, the study of using PLs as separation mediums is still in its preliminary stage [24]. PLs synthesized by MOFs and steric hindrance solvents such as ionic liquids (ILs) have many advantages and become promising candidate coating materials to prepare coated capillary columns for GC and electrochromatography separations. However, the application of PLs as a novel chromatographic separation medium has not been reported yet. Therefore, the development of novel chiral PLs with high enantioselectivity and excellent chiral recognition ability for use in the field of chromatography is of great significance.

Herein, we report the first exploration of using MOF based type III PL D-his-ZIF-8-[Bpy][NTf_2] as a novel stationary phase for high-resolution GC separation of various analytes, including n-alkanes, n-alcohols, aromatic hydrocarbon mixtures, positional isomers, and racemic compounds. The results indicated that the PL has potential application prospect as a new type of stationary phase for GC separation, which will open up a new way for the application of chiral porous frameworks in chromatography.

D-his-ZIF-8 and D-his-ZIF-8-[Bpy][NTf_2] were synthesized with the references [44–46] (Fig. 1). The detailed information is displayed in Supporting information. Fig. S10 (Supporting information) shows photos of porous liquid D-his-ZIF-8-[Bpy][NTf_2] and its corresponding samples after setting for more than two months at room temperature, indicating that the D-his-ZIF-8 nanocrystals can stably suspend in IL [Bpy][NTf_2] for a long time.

Chiral MOF D-his-ZIF-8 nanocrystals and PL D-his-ZIF-8-[Bpy][NTf_2] were characterized using power X-ray diffraction (PXRD), Fourier transform infrared (FT-IR), circular dichroism (CD), Brunauer-Emmett-Teller (BET), thermogravimetric analysis (TGA), and positron (e^+) annihilation lifetime spectroscopy (PALS), while the D-his-ZIF-8-[Bpy][NTf_2] coated capillary column was characterized by the scanning electron microscopy (SEM). The PXRD pattern of the synthesized ZIF-8 (Fig. S1 in Supporting information) was well matched with the simulated pattern, confirming the successful synthesis of ZIF-8 nanocrystals. Furthermore, the characteristic diffraction peaks of the prepared D-his-ZIF-8 nanocrystals were in good agreement with those of ZIF-8, indicating that the crystal structure of D-his-ZIF-8 is consistent with that of ZIF-8. In addition, comparing the PXRD pattern of D-his-ZIF-8 collected by centrifugation and methanol washing from D-his-ZIF-8-[Bpy][NTf_2] with the pattern of D-his-ZIF-8, it was confirmed that D-his-ZIF-8 can stably exist in IL ([Bpy][NTf_2]) without significant changes in crystal structure.

As shown in Fig. S2 (Supporting information), the typical broad absorption band of D-histidine in the range of 3300–2200 cm^{-1} disappeared, and the peak value of N–H stretching vibration of D-histidine at 925 cm^{-1} also disappeared, which indicates that the N–H and carboxyl groups of D-histidine introduced into the framework underwent deprotonation, resulting in the disappearance of N–H and O–H stretching vibrations within this range. The remaining absorption peaks between 3300 and 2200 cm^{-1} belong to the C–H stretching bond. In addition, the absorption peak of D-his-ZIF-8 at 1659 cm^{-1} is attributed to the C=O vibration in D-histidine, which further confirms the successful synthesis of chiral MOF D-his-ZIF-8.

The BET surface area and pore size distribution results for D-his-ZIF-8 and D-his-ZIF-8-[Bpy][NTf_2] are shown in Fig. S3 (Supporting information). The BET of D-his-ZIF-8 collected from D-his-ZIF-8-[Bpy][NTf_2] through centrifugation and methanol washing and synthesized D-his-ZIF-8 was measured by N_2 adsorption/desorption analysis at 77 K, which exhibited a similar typical type I isotherm. In addition, the pore sizes of both D-his-ZIF-8 and D-his-ZIF-8-[Bpy][NTf_2] are mainly distributed at ~1.0 nm, with BET surface areas of 1384.99 m^2/g and 1289.22 m^2/g, respectively. The results show that the [Bpy][NTf_2] cannot enter the cavity of D-his-ZIF-8, and the suspended D-his-ZIF-8 in [Bpy][NTf_2] will maintain its original porosity. Fig. S4 (Supporting information) shows that the pore window size of D-his-ZIF-8 is ~3.4 Å [46], while the molecular size of [Bpy][NTf_2] (*ca.* 19.06 Å × 8.49 Å × 8.11 Å) is larger than the pore opening size of D-his-ZIF-8, which further proved that the [Bpy][NTf_2] with larger molecular size cannot occupy the cavities in ZIF-8.

Table 1
Positron lifetime parameters of D-his-ZIF-8, [Bpy][NTf_2], and D-his-ZIF-8-[Bpy][NTf_2].[a]

Sample	τ_1 (ns)	τ_2 (ns)	τ_3 (ns)	I_1 (%)	I_2 (%)	I_3 (%)
D-his-ZIF-8	0.386	1.719	8.905	77.73	17.94	4.33
IL	0.426	3.205		92.73	7.28	
D-his-ZIF-8-IL	0.427	3.241	0.966	86.78	7.46	5.77

[a] τ: positron (e^+) annihilation lifetime and I: intensity of lifetime.

The TGA determination of D-his-ZIF-8-[Bpy][NTf_2] was performed from 25 °C to 800 °C at 20 °C/min (Fig. S5a in Supporting information). The TGA curve shows that the D-his-ZIF-8-[Bpy][NTf_2] can be stable below 400 °C, indicating that the prepared PL D-his-ZIF-8-[Bpy][NTf_2] with high thermal stability is suitable for usage as a GC stationary phase. The chiral structure of D-his-ZIF-8 was characterized using CD spectroscopy. From Fig. S5b (Supporting information), the D-his-ZIF-8 exhibits a significant negative dichroism signal at 235 nm compared to ZIF-8, confirming the successful insertion of the chiral functional groups into the ZIF-8 framework through self-assembly of Zn^{2+} and double ligands including 2-methylimidazole and D-histidine.

To confirm whether the pores of D-his-ZIF-8 in IL are still empty, D-his-ZIF-8, [Bpy][NTf_2], and D-his-ZIF-8-[Bpy][NTf_2] were characterized through PALS, which is a mature technique for studying hollow pores in materials. In principle, positrons emitted from a positron source, such as Na, will annihilate by interacting with electrons in the material. If there are voids in the material, positrons will reside in the voids and annihilate at a slower rate than in most substances. The positron lifetime can be correlated with the average pore size of the material through a comprehensive model. Fig. S6 (Supporting information) shows the PALS of D-his-ZIF-8, [Bpy][NTf_2], and D-his-ZIF-8-[Bpy][NTf_2]. By comparing the observed positron lifetimes in them, the porosity information of D-his-ZIF-8 in [Bpy][NTf_2] can be obtained.

The positron lifetime parameters of D-his-ZIF-8, [Bpy][NTf_2], and D-his-ZIF-8-[Bpy][NTf_2] are listed in Table 1. The short lifetime of D-his-ZIF-8 ($\tau_1 = 0.386$ ns) is contributed by ligands, and the two longer components ($\tau_2 = 1.719$ ns and $\tau_3 = 8.905$ ns) are attributed to positron annihilation in the small and large pores of D-his-ZIF-8, respectively. The lifetimes of [Bpy][NTf_2] are $\tau_1 = 0.426$ ns and $\tau_2 = 3.205$ ns. In addition, PL D-his-ZIF-8-[Bpy][NTf_2] has three lifetimes, including τ_1 (0.427 ns) and τ_2 (3.241 ns) that match the lifetimes of [Bpy][NTf_2], while the lifetime of τ_3 (0.966 ns) is ascribed to D-his-ZIF-8 in ionic liquid [Bpy][NTf_2]. Finally, the positron lifetime τ_3 (0.966 ns) of D-his-ZIF-8-[Bpy][NTf_2] is approximately equal to the weighted average lifetime τ_m (0.994 ns) of D-his-ZIF-8. Therefore, it can be correctly concluded from PALS data that D-his-ZIF-8 is empty in [Bpy][NTf_2].

The PL coated column was fabricated by static coating method using chiral PL D-his-ZIF-8-[Bpy][NTf_2] as the chiral stationary phase (CSP) and characterized by SEM. It can be obviously seen from Fig. 2 that a uniform coating layer of D-his-ZIF-8-[Bpy][NTf_2] with a thickness of approximately 300 nm was deposited on the inner wall of the capillary column.

Column efficiency is a very important parameter for evaluating the separation performance of chromatographic columns. The Golay curve of column A and column B was evaluated by measuring the height equivalent to a theoretical plate (HETP) of n-dodecane at different flow rates at 120 °C. In Fig. S7 and Table S1 (Supporting information), the minimum HETP of column A (0.32 mm) is lower than that of column B (0.55 mm). This result indicates that column A (3100 plates/m) has higher column efficiency than column B (1850 plates/m). As depicted in Fig. 2 and Fig. S8 (Supporting information), the higher column efficiency of the column A is mainly attributed to the formation of a uniform coating on the inner wall of the capillary. In contrast, Fig. S8 shows that D-his-ZIF-8 nanoparticles aggregate on the inner wall of column B, resulting in poor coating performance. In addition, the McReynolds constant is used to evaluate the polarity of the stationary phase. Benzene, 1-butanol, 1-nitropropane, pyridine, and 2-pentanone were selected as analytes for determination on the column A and column B. Table S2 (Supporting information) lists the McReynolds constants of five analytes with an average value of 213 and 246, which illustrate that the D-his-ZIF-8-[Bpy][NTf_2] and D-his-ZIF-8 CSPs belongs to moderate polarity.

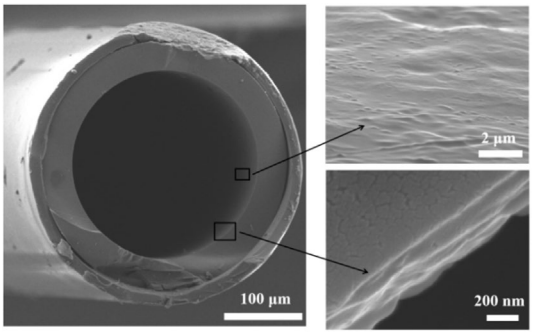


Fig. 2. SEM images of the cross section view and inner surface of D-his-ZIF-8-[Bpy][NTf_2] coated capillary column.

To investigate the separation performance of column A, different types of compounds including *n*-alkanes, *n*-alcohols, and alkylbenzenes were selected as analytes for separation on the column A. Among them, alkanes are an important component of petroleum, and the separation of alkanes is a very important step in petroleum refining. In addition, benzene series are an important industrial raw material for petroleum and chemical industry, as well as a strong carcinogen identified by the World Health Organization. Therefore, the detection and analysis of them is of great significance.

As shown in Fig. 3, the column A provides baseline separation of eight *n*-alkanes, eight *n*-alcohols, and five alkylbenzenes with sharp peak shapes, respectively. Among them, the highly polar compounds such as *n*-alcohols do not have obvious tails in chromatographic separation. The high-resolution separation of different types of organic compounds is mainly attributed to the van der Waals forces, hydrogen bonds, or π-π interactions between analytes and D-his-ZIF-8-[Bpy][NTf_2] stationary phase. Meanwhile, the commercial HP-35 column was employed for comparison. As shown in Fig. S11 (Supporting information), the elution order of *n*-alkanes, *n*-alcohols, and alkylbenzens on column A is identical to that on the HP-35 column. Moreover, the separation efficiency of column A is equivalent to that of HP-35 column. The results indicates that the D-his-ZIF-8-[Bpy][NTf_2] coated capillary column has potential application for GC separation of homologous mixtures.

The separation of isomers with similar physicochemical properties is still a challenging issue. In this study, column A has a good selectivity for the separation of positional isomers (dichlorobenzene, dibromobenzene, and nitrobromobenzene), structural isomers (α-, β-ionone), and *cis-trans* isomers (nerol/geraniol, and 1,3-dichloropropene). The chromatograms of the six isomers on column A are shown in Fig. 4 and the chromatographic data are listed

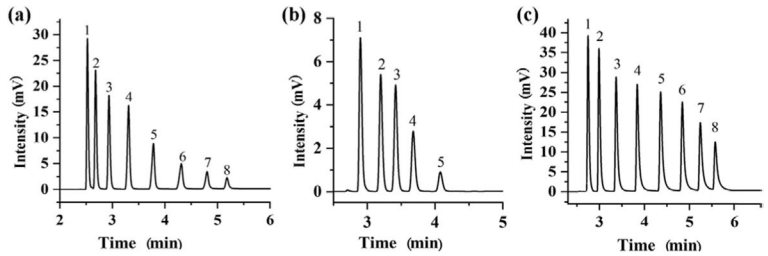


Fig. 3. GC chromatograms on the column A (15 m length × 0.25 mm i.d.) for the separation of (a) *n*-alkanes mixture (1–8: *n*-octane, *n*-nonane, *n*-decane, *n*-undecane, *n*-dodecane, *n*-tridecane, *n*-tetradecane, and *n*-pentadecane in turn), heating procedure: 50 °C for 1.5 min, then heated to 182 °C at 53 °C/min, N_2 linear velocity: 21.0 cm/s; (b) alkylbenzens mixture (1–5: benzene, toluene, ethylbenzene, *n*-propylbenzene, and *n*-butylbenzene), heating procedure: 90 °C for 1.5 min, then heated to 190 °C at 40 °C/min, N_2 linear velocity: 20.5 cm/s; (c) *n*-alcohols mixture (1–8: ethanol, 1-propanol, 1-butanol, 1-pentanol, 1-hexanol, 1-heptanol, 1-octanol and 1-nonanol), heating procedure: 70 °C for 1.5 min, then heated to 210 °C at 60 °C/min, N_2 linear velocity: 20.5 cm/s.

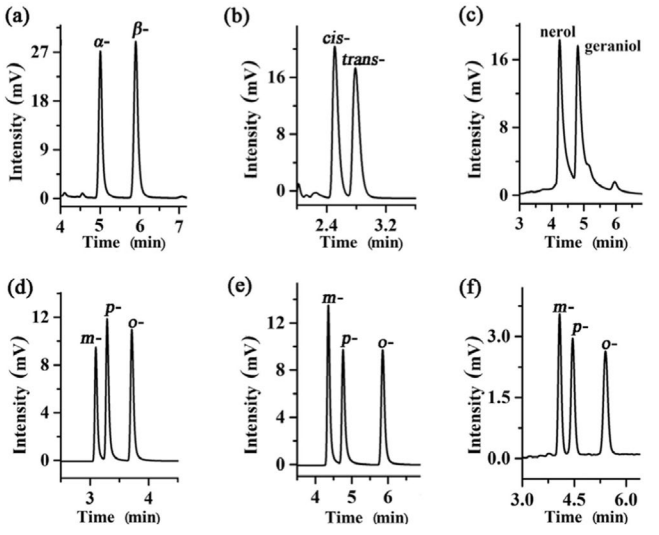


Fig. 4. GC chromatograms on the column A for the separation of (a) *α*-, *β*-ionone; (b) 1,3-dichloropropene; (c) nerol, geraniol; (d) *o*-, *m*-, *p*-dichlorobenzene; (e) *o*-, *m*-, *p*-dibromobenzene; (f) *o*-, *m*-, *p*-nitrobromobenzene. The chromatographic conditions are shown in Table S2.

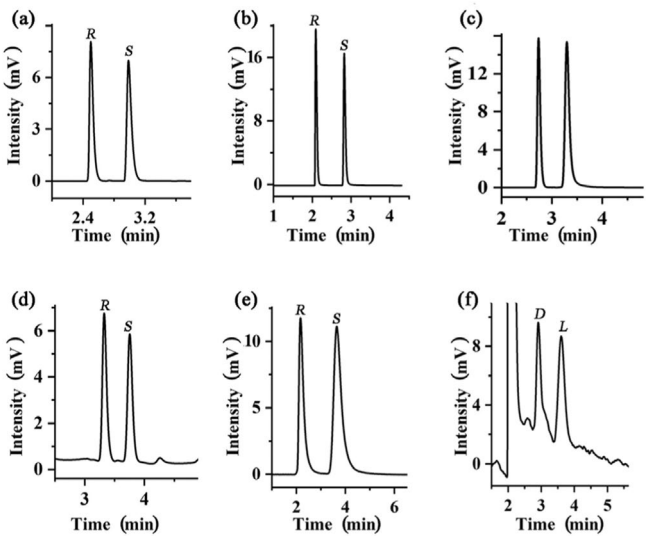


Fig. 5. Typical GC chromatograms obtained on the column A for separation of racemic compounds: (a) 3-butyne-2-ol; (b) 2-butanol; (c) *γ*-nonolactone; (d) 2-methyltetrahydrofuran-3-one; (e) ethyl lactate; and (f) tyrosine derivative. The chromatographic conditions as shown in Table 2.

in Table S3 (Supporting information). Compared with the commercial HP-35 column (Fig. S12 in Supporting information), column A demonstrates comparable separation performance for most isomers, except for nerol/geraniol. Moreover, the previously reported P5A-C10–2NH_2 column was also used for comparison [47]. In Fig. S13 (Supporting information), the separation effect of three positional isomers and nerol/geraniol on column A is slightly superior to that on the P5A-C10–2NH_2 column, except for nerolidol/geraniol. The results indicate that the column A is practical for chromatographic separation.

In order to evaluate the resolution ability of D-his-ZIF-8-[Bpy][NTf_2], fifteen pairs of enantiomers were separated on the column A, including 3-butyne-2-ol, 2-butanol, *γ*-nonolactone, 2-methyltetrahydrofuran-3-one, ethyl lactate, methyl 2-chloropropionate, methyl 2-bromobutyrate, styrene oxide, 2-phenylpropionaldehyde, ethyl 2-bromobutyrate, 2-iodobutane, 3–chloro-2-butanone, isoleucine derivative, tyrosine derivative, and valine derivative. These racemic compounds include alcohols, esters, epoxides, ketones, halogenated hydrocarbons, and amino acid derivatives. The separation factors (*α*), resolutions (*Rs*), and column temperatures (*T*) are listed in Table 2, and the chromatograms are shown in Fig. 5 and Fig. S9 (Supporting information). As shown in Fig. 5 and Fig. S9, and Table 2, the chiral PL D-his-ZIF-8-[Bpy][NTf_2] as novel a GC stationary phase exhibits high enantioselectivity and good separation performance towards various types of racemic compounds. Nearly half of the racemic compounds achieved baseline separation with sharp peaks on the column A, and the maximum resolution value of 2-butanol can reach 7.36.

Compared the separation performance of column A with D-his-ZIF-8 coated column B, the comparison results of the two capillary columns for the separation of these enantiomers are shown in Table 2. The resolution chromatograms of enantiomers are shown in Fig. S14 (Supporting information). The resolution values of enantiomers on the column A are higher than those on the column B. Obviously, the separation performance of column A is significantly better than that of column B, indicating that chiral porous liquid D-his-ZIF-8-[Bpy][NTf_2] as a new stationary phase exhibits excellent chiral resolution ability and practical application potential in capillary GC.

On the surface of D-his-ZIF-8, there are abundant amount of reactive Zn^{2+} ions and D-histidine species. These superficial $Zn^{2+}$and amino or carboxyl groups of D-histidine from adjacent particles could bond each other, which will cause aggregation between crystal particles and hinder the interaction between analyte molecules and D-histidine. However, in D-his-ZIF-8-[Bpy][NTf_2] PL, the interaction between D-his-ZIF-8 and [Bpy][NTf_2] IL based on electrostatic interaction can greatly decrease the aggregation between nanocrystalline particles and the adsorption effect of Zn^{2+} on analyte molecules, which also facilitates the chiral recognition be-

Table 2
Separation of racemic compounds on the D-his-ZIF-8-[Bpy][NTf_2] coated capillary column (column A), D-his-ZIF-8 coated capillary column (column B), and β-DEX 120 column (column C).

Racemates	D-his-ZIF-8-[Bpy][NTf_2] coated column (column A)				D-his-ZIF-8 coated column (column B)				β-DEX 120 column (column C)			
	T (°C)	α	Rs	V (cm/s)[a]	T (°C)	α	Rs	V (cm/s)[a]	T (°C)	α	Rs	V (cm/s)[a]
3-Butyne-2-ol	70	1.37	4.94	12.5	80	1.17	1.80	13.5	65	1.09	3.46	12.5
2-Butanol	140	1.84	7.36	16.5	155	1.15	1.25	13.8	50	1.04	1.35	12.8
γ-Nonolactone	160	1.48	4.33	13.2	130	1.08	1.36	12.6	150	1.01	0.81	14.3
2-Methyltetrahydrofuran-3-one	175	1.24	2.92	12.8	185	1.02	1.35	13.1	65	1.03	1.60	14.3
Ethyl lactate	120	2.53	1.80	15.6	130	1.09	1.20	15.1	100	1.00	-[c]	13.8
Methyl 2-chloropropionate	145	1.11	1.34	13.5	150	1.03	0.80	14.1	85	1.06	2.76	13.5
Methyl 2-bromobutyrate	120	2.44	1.38	14.7	130	1.08	0.72	12.6	110	1.05	2.10	14.2
Styrene oxide	130	1.41	1.39	13.1	110	1.02	0.65	14.8	115	1.03	1.92	14.3
2-Phenylpropionaldehyde	130	1.17	1.12	11.9	160	1.05	0.59	14.5	125	1.00	-[c]	13.2
Ethyl 2-bromobutyrate	160	1.11	1.43	13.8	140	1.00	-[c]	12.9	115	1.03	1.72	14.2
2-Iodobutane	170	1.09	0.84	15.6	160	1.14	0.40	14.5	70	1.00	-[c]	12.5
3-Chloro-2-butanone	130	1.36	0.93	16.6	145	1.08	0.50	14.7	65	1.02	0.91	12.5
Isoleucine[b]	140	1.05	1.01	11.1	135	1.00	-[c]	14.0	95	1.02	1.03	15.0
Tyrosine[b]	150	1.55	1.71	12.3	145	1.01	0.88	13.0	175	1.00	-[c]	13.9
Valine[b]	90	1.66	1.75	20.6	100	1.00	-[c]	16.0	95	1.00	-[c]	14.2

[a] V is the linear velocity of carrier gas of N_2; [b] Trifluoroacetyl isopropyl ester derivatives; [c] Cannot be separated. Column A and column B: 15 m length × 0.25 mm i.d.; column C: 30 m length × 0.25 mm i.d.

tween analyte molecules and D-histidine. In addition, compared to D-his-ZIF-8 solid particles, the D-his-ZIF-8-[Bpy][NTf_2] PL stationary phase has better coating performance and mass transfer effect. Therefore, the above mentioned phenomena will help improve the column efficiency and separation performance of D-his-ZIF-8-[Bpy][NTf_2] coated column, which is also the main reason that the separation effect of this column is better than that of pure MOF coated column.

In addition, the chiral recognition ability of column A and the commercially available β-DEX120 column (column C) was compared. The separation data and comparative chromatograms of fifteen pairs of enantiomers on column A and column C are shown in Table 2 and Fig. S15 (Supporting information), respectively. From Table 2, five pairs of enantiomers, including ethyl lactate, 2-phenylpropionaldehyde, 2-iodobutane, tyrosine derivative, and valine derivative, that cannot be separated on column C, but can be separated on column A. Furthermore, ten pairs of enantiomers can be separated on column C, among which five pairs of enantiomers (3-butyne-2-ol, 2-butanol, γ-nonolactone, 2-methyltetrahydrofuran-3-one, and 3–chloro-2-butanone) have higher resolution values on the column A than on the column C. The enantioselectivity of column A for some alcohols, esters, and ketones is higher than that of column C. However, methyl 2-chloropropionate, methyl 2-bromobutyrate, styrene oxide and ethyl 2-bromobutyrate achieved baseline separation on column C with higher resolution values than column A, indicating that the chiral recognition ability of column A can be complementary to that of column C.

D-his-ZIF-8-[Bpy][NTf_2] coated column showed good recognition ability for racemates, which was related to the chiral microenvironment of D-his-ZIF-8-[Bpy][NTf_2]. The separation mechanism between chiral analytes and CSPs is difficult to explain in detail. From Fig. 5 and Fig. S9, it can be observed that the different elution order of enantiomers and amino acid derivatives on column A. For example, for the separation of chiral alcohols and amino acid derivatives, the enantiomers of chiral alcohols are eluted after their *(R)*-enantiomers, while the L-configuration of chiral amino acid derivatives are eluted after their D-configuration, demonstrating that D-his-ZIF-8-[Bpy][NTf_2] has stronger interaction with (*S*)-enantiomers for chiral alcohols and L-configuration for amino acid derivatives, respectively. The process of chiral recognition between chiral D-his-ZIF-8-[Bpy][NTf_2] and enantiomer molecules is

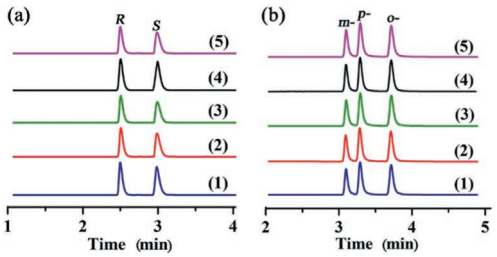


Fig. 6. GC chromatograms on the column A for five replicate separation of (a) 3-butyne-2-ol at a N_2 flow rate of 14.5 cm/s under 70 °C and (b) *o,m,p*-dichlorobenzene at a N_2 flow rate of 16.7 cm/s under 150 °C. (1): Chromatograms obtained from the initial use of the column; (2) and (3): chromatograms obtained after the column was undergone 200 and 400 injections, respectively; (4) and (5): chromatograms obtained after the column was conditioned at 250 °C for 5 h and 10 h, respectively.

mainly ascribed to host-guest interaction and chiral spatial coordination. Multiple interactions may be involved, including hydrogen-bondings, π-π interactions, dispersion forces, and dipole-dipole interactions, as well as the formation of stable symmetric zeolite topologies in D-his-ZIF-8 porous crystal materials that can also promote chiral recognition processes. In particular, the N or H atoms of amino groups in the D-his-ZIF-8 framework are prone to form hydrogen-bonding interactions with chiral compounds such as chiral alcohols and amino acid derivatives, which may be related to the exposed D-histidine structure on the surface. Therefore, this chiral column exhibits excellent resolution performance for alcohols, indicating that hydrogen bond interactions play a very important role in the recognition process of chiral alcohols. In addition, D-his-ZIF-8-[Bpy][NTf_2] coated capillary column has good separation performance towards esters and ketones, including γ-nonolactone, 2-methyltetrahydrofuran-3-one, ethyl lactate, methyl 2-chloropropionate, methyl 2-bromobutyrate, and ethyl 2-bromobutyrate, which may indicate that dipole-dipole interactions also participate in resolution process.

To investigate the reproducibility and stability of column A, 3-butyne-2-ol and dichlorobenzene were selected as the analytes for repeated injection separation on the chiral column. Fig. 6 shows the chromatograms of repeated separation of 3-butyne-2-ol and dichlorobenzene after the column undergone multiple injections

used and high temperature conditioned. It can be observed that there are no significant changes in retention time, selectivity, and separation performance. The relative standard deviations (RSDs) of the retention time and peak area of the two analytes were <1.80% and 0.80%, respectively. The results showed that the D-his-ZIF-8-[Bpy][NTf_2] coated capillary column has good reproducibility and stability for GC separation of enantiomers and isomers.

To examine the practicability of column A for real samples, we employed it for the determination of enantiomeric excess (*ee*) in commercial reagent samples and asymmetric catalytic products. Fig. S16 (Supporting information) shows the chromatograms for the separation of commercial reagent samples ((*R*)-3-butyne-2-ol and (*S*)-2-butanol) and asymmetric catalytic product (styrene oxide) on the column A, respectively. According to the calculation formula for *ee* value, their *ee* values were 98.7%, 98.2%, and 56.3%, respectively, showing good accordance with their labeled enantiopurities ((*R*)-3-butyne-2-ol, $ee \geq 98\%$; (*S*)-2-butanol, $ee \geq 98\%$) and the *ee* value of styrene oxide ($ee = 57\%$) obtained by enantioselective catalytic epoxidation in the reference [48]. The above-mentioned results for real samples demonstrate the great potential of column A for practical GC applications.

In conclusion, we first report the application of a type III chiral porous liquid D-his-ZIF-8-[Bpy][NTf_2] for high-resolution GC separation. The D-his-ZIF-8-[Bpy][NTf_2] coated capillary column exhibited high selectivity and excellent separation performance with good reproducibility for *n*-alkanes, *n*-alcohols, alkylbenzens, and isomers, especially for racemic compounds, including esters, ketones, epoxides, alcohols, halohydrocarbons, and amino acid derivatives. The chiral resolving ability of D-his-ZIF-8-[Bpy][NTf_2] coated capillary column is superior to the prepared D-his-ZIF-8 coated capillary column. In addition, the chiral recognition ability of D-his-ZIF-8-[Bpy][NTf_2] column is complementary to that of commercially available β-DEX 120 column, which can separate some racemates that could not be separated on β-DEX 120 column. This research results indicate that chiral porous liquid D-his-ZIF-8-[Bpy][NTf_2] based on chiral MOF as a novel stationary phase offered excellent chromatographic separation performance, which will open up a new way for the practical application potential of porous solid materials in the field of chromatography. However, many porous framework materials tend to undergo structural collapse or self-filling in liquid environments, leading to reduced porosity. Moreover, it is a challenge to enhance the fluidity of PLs while maintaining their permanent porosity. Therefore, the future research should focus on identifying more suitable porous materials and hinder solvents to develop novel PLs with superior properties (such as high porosity and good fluidity) for use in separation field.

Declaration of competing interest

The authors declare that they have no known competing financial interests or personal relationships that could have appeared to influence the work reported in this paper.

CRediT authorship contribution statement

Xiao-Yan Ran: Writing – original draft, Software, Data curation, Conceptualization. **Tian-Jian Xiong:** Writing – original draft, Software, Methodology, Investigation. **Yu-Ping Yang:** Software, Resources. **Zong-Hong Luo:** Validation, Formal analysis. **Cheng Liu:** Software, Data curation. **Yu-Lan Zhu:** Validation, Formal analysis. **Jun-Hui Zhang:** Validation, Funding acquisition, Formal analysis. **Bang-Jin Wang:** Writing – review & editing, Resources. **Sheng-Ming Xie:** Writing – review & editing, Writing – original draft, Supervision. **Li-Ming Yuan:** Supervision.

Acknowledgments

This work was supported by the National Natural Science Foundation of China (Nos. 22364022, 22064020, and 21964021) and the Applied Basic Research Foundation of Yunnan Province (Nos. 202101AT070101 and 202201AT070029).

Supplementary materials

Supplementary material associated with this article can be found, in the online version, at doi:10.1016/j.cclet.2025.111864.

References

[1] C. He, Y.H. Zou, D.H. Si, et al., Nat. Commun. 14 (2023) 3317.
[2] S.L. James, Adv. Mater. 28 (2016) 5712–5716.
[3] C.M. Corrêa, J. Avila, T. El Achkar, et al., Chem. Commun. 61 (2025) 5818–5821.
[4] X.Q. Li, D.C. Wang, Z.J. He, et al., Chem. Eng. J. 417 (2021) 129239.
[5] M.K. Dinker, K. Zhao, S. Liu, et al., J. Mater. Chem. A 10 (2022) 16204–16211.
[6] N. Giri, M.G. Del Popolo, G. Melaugh, et al., Nature 527 (2015) 216–220.
[7] J.S. Zhang, S.H. Chai, Z.A. Qiao, et al., Angew. Chem. Int. Ed. 54 (2015) 932–936.
[8] J.H. Wang, L. Avram, Y. Diskin-Posner, et al., J. Am. Chem. Soc. 144 (2022) 21244–21254.
[9] K.C. Jie, Y.J. Zhou, H.P. Ryan, et al., Adv. Mater. 33 (2021) 2005745.
[10] A. Bavykina, A. Cadiau, J. Gascon, Coord. Chem. Rev. 386 (2019) 85–95.
[11] A.T. Kai, B.D. Egleston, A. Tarzia, et al., Adv. Funct. Mater. 31 (2021) 2106116.
[12] K.C. Jie, N. Onishi, J.A. Schott, et al., Angew. Chem. Int. Ed. 59 (2020) 2268–2272.
[13] P.F. Fulvio, S. Dai, Chem 6 (2020) 3263–3287.
[14] L. Ma, C.J.E. Haynes, A.B. Grommet, et al., Nat. Chem. 12 (2020) 270–275.
[15] N. O'Reilly, N. Giri, S.L. James, Chem. Eur. J. 13 (2007) 3020–3025.
[16] D.C. Wang, Y.Y. Xin, X.Q. Li, et al., Chem. Eng. J. 416 (2021) 127625.
[17] Y.J. Zhou, K.C. Jie, Chin. Chem. Lett. 36 (2025) 111007.
[18] L. Errui, G. Arvind, L.Q. Qiu, et al., Adv. Funct. Mater. 35 (2025) 2413668.
[19] W.J. Li, S.Y. Mukherjee, Natl. Sci. Rev. 12 (2025) nwaf075.
[20] S.Q. Li, D.X. wang, Y.J. Lee, et al., Angew. Chem. Int. Ed. 63 (2024) e202405288.
[21] H.S. Ma, X.Q. Ju, B.L. Cui, et al., ACS Appl. Mater. Interfaces 17 (2025) 13836–13850.
[22] X.Q. Li, D.C. Wang, Z.J. He, J. Mater. Chem. A 10 (2022) 13333–13344.
[23] Y.H. Zou, Y.B. Huang, D.H. Si, et al., Angew. Chem. Int. Ed. 60 (2021) 20915–20920.
[24] Y. Wang, Y.W. Sun, H. Bian, et al., ACS Appl. Mater. Interfaces 12 (2020) 45916–45928.
[25] Y. Liu, H.Y. Jin, M.M. Li, et al., Angew. Chem. Int. Ed. 64 (2025) e202501191.
[26] P.W. Wu, B.Z. Wang, L.L. Chen, et al., Adv. Sci. 11 (2024) 2401996.
[27] R.B. Dennis, M.J. Hurlock, T.M. Nenoff, et al., ACS Appl. Mater. Interfaces 17 (2025) 5496–5505.
[28] J. Yin, W.D. Fu, J.R. Zhang, et al., Chem. Eng. J. 470 (2023) 144290.
[29] H.L. Ning, X.Y. Ge, L.S. Sheng, et al., Adv. Mater. 37 (2025) 2417106.
[30] T. Huang, X.Y. Lei, S.Q. Wang, et al., J. Chromatogr. A 1692 (2023) 463849.
[31] Y. Wang, Z. Feng, Y.W. Sun, et al., Soft Matter 18 (2022) 975–982.
[32] P.P. Li, J.A. Schott, J.S. Zhang, et al., Angew. Chem. Int. Ed. 56 (2017) 14958–14962.
[33] E.B. Hemming, A.F. Masters, T. Maschmeyer, Chem. Eur. J. 26 (2020) 7059–7064.
[34] C. Zeng, H. Yang, M. Xu, et al., Chin. Chem. Lett. 37 (2026) 110064.
[35] C. Yuan, Z. Wang, W.Q. Xiong, et al., J. Am. Chem. Soc. 145 (2023) 18956–18967.
[36] B. Tang, W. Wang, H.P. Hou, et al., Chin. Chem. Lett. 33 (2022) 898–902.
[37] T. Sun, Y. Zhang, H. Liu, et al., Talanta 283 (2024) 127098.
[38] T. Sun, R.N. Chen, Q.C. Huang, et al., ACS Appl. Mater. Interfaces 14 (2022) 56132–56142.
[39] G.L. Sun, Y.C. Luo, Z.H. Yan, et al., Chin. Chem. Lett. 35 (2024) 109787.
[40] H.L. Qian, C.X. Yang, X.P. Yan, et al., Nat. Commun. 7 (2016) 12104.
[41] P.P. Li, H. Chen, J.A. Schott, et al., Nanoscale 11 (2019) 1515–1519.
[42] L. Errui, M.S. Kevin, Z.Z. Yang, et al., Chem. Sci. 15 (2024) 17720–17738.
[43] H. Mahdavi, N.T. Eden, C.M. Doherty, et al., ACS Appl. Mater. Interfaces 14 (2022) 23392–23399.
[44] J.Y. Chan, H.C. Zhang, Y. Nolvachai, et al., Angew. Chem. Int. Ed. 57 (2018) 17130–17134.
[45] X.S. Wang, Y.A. Zhu, J. Liu, et al., Chem. Asian J. 13 (2018) 1535–1538.
[46] S.J. Liu, J.D. Liu, X.D. Hou, et al., Langmuir 34 (2018) 3654–3660.
[47] T. Sun, Q.C. Huang, W. Zhang, et al., J. Chromatogr. A 1671 (2022) 463008.
[48] W. Zhang, J.L. Loebach, S.R. Wilson, et al., J. Am. Chem. Soc. 112 (1990) 2801–2803.